SWIPT aided Cooperative Communications with Energy Harvesting based Selective-Decode-and-Forward Protocol: Benefiting from Channel Aging Effect

Yali Zheng, Jie Hu, *Senior Member, IEEE* and Kun Yang, *Fellow, IEEE*

***Abstract*—Simultaneous wireless information and power transfer (SWIPT) in radio-frequency (RF) bands enables flexible deployment of battery-powered relays for extending communication coverage. Relays receive downlink RF signals emitted by a source for information decoding and energy harvesting, while the harvested energy is consumed for both information decoding and information forwarding to a destination. An energy harvesting based selective-decode-and-forward (EH-SDF) protocol is proposed, where only the relays having information correctly decoded are activated for information forwarding, while others harvest and store energy for the future use. By considering the channel aging effect, we propose a joint relay selection, power allocation, transmit beamforming and signal splitting design in order to maximise the end-to-end (e2e) throughput of this EH-SDF aided cooperative communication system. Two scenarios with/without direct link between the source and the destination are studied, respectively. The original formulated non-convex optimisation problems with coupled variables are decoupled into three subproblems which are solved by an iterative optimisation algorithm. Numerical results demonstrate that our design with the EH-SDF protocol achieves a higher e2e throughput than the traditional decode-and-forward (DF) counterpart. Moreover, the impact of the channel aging effect on the e2e throughput is also evaluated.**

***Index Terms*—Simultaneous wireless information and power transfer (SWIPT), cooperative communication, selective-decode-and-forward (SDF), energy harvesting, channel aging effect**

I. Introduction

A. Background

Nowadays, a huge number of battery-powered or batteryless communication devices are being deployed for accommodating various exciting applications such as smart transportation, smart industry, smart health-care, smart agriculture and etc., which constitutes a promising future of smart cities. Generally, these communication devices are classified into two categories: low-power terminals for sensing and data collections, such as sensors and other Internet of Things (IoT) devices [1], and low-power 'infrastructure' for extending communication coverage, such as relay stations [2] and mobile stations (e.g. drones) [3]. Functions of these devices are largely constrained by their limited battery capacity. Thankfully, wireless power transfer (WPT) in radio-frequency (RF) bands is capable of addressing this dilemma by largely extending the lifespan of these devices [4]. In order to accommodate the coexistence of WPT and conventional wireless information transfer (WIT) in the same RF band, simultaneous wireless information and power transfer (SWIPT) has emerged as a promising technique [5].

Due to the serious path-loss after a long propagation distance, the received RF signal power at receivers is too weak to be relied upon for information decoding. Therefore, relay stations are deployed for effectively extending the coverage of centralised infrastructure, such as base-stations (BSs) and access-points (APs) [6]. By exploiting the SWIPT technique, relay stations become energy self-sustainable [7]. They are capable of harvesting energy and decoding information from the downlink transmissions of centralised infrastructure by splitting the received RF signals either in the power-domain [8] or in the time domain [9]. The information forwarding can also be powered by the energy harvested by relay stations [8]–[14]. As a result, light-weighted relay stations are available for quickly eliminating coverage hole and for timely communication recovery in emergency scenarios.

Normally, either the amplify-and-forward (AF) or the decode-and-forward (DF) protocol can be adopted by these light-weighted relays in order to forward received information to destinations [10]. When the AF protocol is adopted by relays, some of precious energy harvested is consumed for amplifying and forwarding useless noises and interferences to destinations, which substantially degrades end-to-end (e2e)

The authors would like to thank the financial support of National Natural Science Foundation of China (No. 61971102, 62132004), MOST Major Research and Development Project (No. 2021YFB2900204), Sichuan Major R&D Project (No. 22QYCX0168), Sichuan Science and Technology Program (No. 2022YFH0022). (*Corresponding author: Jie Hu.*)

Yali Zheng, Jie Hu and Kun Yang are with the School of Information and Communication Engineering, University of Electronic Science and Technology of China, Chengdu, China, 611731, email: yalizheng@std.uestc.edu.cn, hujie@uestc.edu.cn, kyang@ieee.org.

Kun Yang is also with the Yangtze Delta Region Institute, University of Electronic Science and Technology of China, Quzhou, China, 324000.

performance and results in low energy-efficiency [15]. By adopting the DF protocol, useful information is firstly decoded at relays. Therefore, harmful noises and interferences received at relays are effectively removed. No additional energy is consumed for forwarding these useless part of received signals [11]–[14].

However, in a conventional DF protocol, relays never check transmission errors during their information decoding, which may result in error propagation in the subsequent information forwarding stage. Furthermore, most works only considered a single SWIPT aided relay in cooperative communication systems, the potential diversity gains introduced by multiple relays have been ignored [16]. Recently, a novel selective-decode-and-forward (SDF) protocol was proposed for overcoming the drawbacks of the conventional DF in a multi-relay based cooperative communication system [17]. Relays are activated for forwarding decoded information, only when their decoded information has no error. Furthermore, we propose an energy harvesting based SDF (EH-SDF) protocol for multi-relay based cooperative communications with the aid of SWIPT. In this protocol, the inactive relays with information decoding errors are only allowed to harvest energy for replenishing their batteries. Therefore, they may gain more energy for forwarding information in the following transmission frames (TFs).

Moreover, most works on the SWIPT-aided relay communication networks considered a block-fading model, i.e., the channel state information (CSI) is assumed to be a constant in a coherence transmission block. However, its drawback is two-fold: First, frequent channel estimation is unpractical at the SWIPT-aided relay due to the additional energy consumption for transmitting training pilots and CSI feedback. Second, channel estimation is carried out before source nodes transmit the information signal to relays during the 1st-hop transmission, which results in the outdated CSI during the 2nd-hop transmission owing to the time-varying characteristic of the channel. However, in practice, channel states in subsequent TFs are correlated to one another. This is called the channel aging effect [18]. By considering this effect, we may realise optimal transmission design in both hops from the source to the SWIPT-aided relays and finally to the destination.

B. Related Works

Nowadays, there are plenty of works focusing on WPT/SWIPT aided cooperative communications. Specifically, Oshaghi *et al.* [11] maximised e2e throughput in a SWIPT aided DF cooperative system with a single relay by optimising the power splitting ratio and the power allocation at both the source and the relay. A WPT/SWIPT-aided cooperative communication network with a DF protocol was considered in [12]. By considering the time switching based and the power splitting based protocols, the mutual information was maximised by jointly optimising the covariance matrices of the source and the relay, the time allocation and the power splitting schemes. Moreover, Hu *et al.* [13] focused on ultra-low-latency transmissions in a SWIPT aided DF cooperative system. However, [11]–[13] ignored the energy consumption of decoding at relays. Therefore, Abedi *et al.* [14] considered that energy harvested by a relay is consumed for both information decoding and information forwarding, where they optimised the power splitting ratio for maximising the attainable e2e throughput. Chen *et. al* [19] studied the resource allocation in a wireless cooperative IoT network, where a single relay powered by renewable energy havested is implemented for simultaneously forwarding information to a destination and for wireless charging multiple IoT devices. Li *et. al* [20] investigated a SWIPT based cooperative secure communication system, where a relay simultaneously fowarded information to a destination and injected artificial noise to interfer eavesdroppers. The robust beamforming design was obtained for maximising the secrecy throughput with imperfect channel knowledge. In addition, Liu *et. al* [21] studied a cooperative SWIPT system by implementing multiple full-duplex AF relays with stable energy supply, which aims for SWIPT towards multiple destinations. A wireless powered relay aided communication network was considered in [22]. By considering AF and DF protocols, age of information (AoI) was studied by analysing the statistical characteristics of the channels. Moreover, a joint design on optimal beamforming, antenna selection, time allocation and relay selection was proposed for maximising the intra-frame transmission rate in a WPT/SWIPT aided AF cooperative system [23]. However, the existing works [11]–[14], [19]–[23] did not consider the channel aging effect.

Compared to the DF protocol, SDF aided relays can avoid forwarding incorrect information to destinations, so as to improve system performance. After being invented in [24], the SDF protocol has gained a wide interest in cooperative communications. A number of works have been done for improving the performance of the SDF protocol. For example, Alves *et. al* [25] innovatively let a single relay to accumulate several packets. These packets were then concatenated and forwarded together, which substantially increased the spectrum efficiency. Bouteggui *et. al* [26] invoked the SDF protocol in a MIMO aided cooperative communication system, where they jointly designed the antennas and transmission paths selection scheme in order to maximise the e2e throughput. Yao *et. al* [27] analysed the symbol-error-probability (SEP) of the SDF protocol in a satellite-terrestrial wireless network with multiple relays. All of the above works demonstrate the advantage of the SDF protocol over the classic DF counterpart.

However, the existing works [17], [24]–[27] ignored the inherent nature of the SDF protocol in terms of energy-saving and its potential application with SWIPT. Therefore, we pro-

pose the EH-SDF protocol for multi-relay based cooperative communications with the aid of SWIPT. Its benefits are two-fold: First of all, compared to the DF protocol, an EH-SDF aided relay can avoid forwarding incorrect information to destinations, so as to increase its energy-efficiency. Second, when multiple relays exist, according to the EH-SDF protocol, only the relays receiving correct information are activated for the information forwarding. The inactive relays are capable of harvesting and storing more energy in the current TF, which is beneficial for the information forwarding in the subsequent TFs.

C. Contributions

In order to overcome the drawbacks of the existing works on SWIPT aided cooperative communications, our novel contributions are summarised as follows:

- We study a cooperative communication system with multiple battery-powered relays by considering the existence/non-existence of the direct link between the source and the destination. These relays simultaneously harvest energy and decode information from the downlink RF signals transmitted by a source. Only the relays correctly decoding the information may be activated to forward the information to a destination, so as to reduce the energy consumption, while others only harvest and store energy for the future use. This is our proposed EH-SDF protocol.
- Average e2e throughput is maximised over a range of consecutive TFs by considering channel aging effect. Only the perfect CSI of the very first TF in this range can be acquired. It may address the difficulties of acquiring timely CSI in the two-hops transmission of the cooperative communication.
- Relay selection, transmit beamformers of the source and the relays, the power splitters and the power allocation of the relays are jointly designed with partial CSI by an iterative optimisation algorithm, which is constrained by the energy causality. Specifically, the integer programming subproblem for relay selection is solved by considering two strategies, partial relay selection and max-min relay selection, while the other two subproblems for solving continuous variables are optimally solved, respectively.
- Numerical results demonstrate the fast convergence of our joint design and the advantage of the EH-SDF protocol over the classic DF counterpart in SWIPT based cooperative communication systems. The impact of partial CSI knowledge, i.e., channel aging effect on the performance is also evaluated.

The rest of the paper is organised as follows: After introducing the system model and the problem formulation in Sections II-III, respectively, our joint design is investigated in Section IV. After presenting numerical results in Section V, we conclude our paper in Section VI.

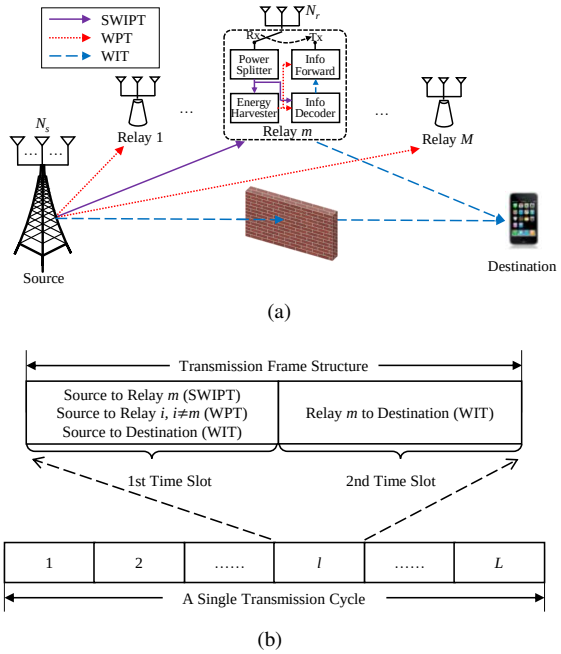

Fig. 1. (a) System model and (b) transmission cycle and transmission frame structure of the downlink SWIPT-CCN with a direct link.

Notations: a represents a scalar; $\mathbf{a}$ represents a vector; $\mathbf{A}$ represents a matrix; $\mathcal{A}$ represents a set; $\mathbf{A}^{\dagger}$ is the conjugate transpose of $\mathbf{A}$; $\mathrm{Tr}(\mathbf{A})$ is the trace of $\mathbf{A}$; $|\mathcal{A}|$ is the cardinality of $\mathcal{A}$.

II. System Model

A. Network Model

The SWIPT aided cooperative communication network (SWIPT-CCN) is illustrated in Fig. 1 (a), which consists of a single source node, a set of cooperative relays $\{m|\forall m = 1, 2, \cdots, M\}$ and a single destination node. The source equipped with N_s antennas transmits the modulated RF signals to the relays and the destination simultaneously in the downlink.

The relays equipped with N_r antennas operating in a half-duplex (HD) mode adopt an EH-SDF protocol, in which they may be activated to forward information only when the information is correctly decoded, otherwise, they only harvest and store energy. They have the following functions:

- *Signal reception:* These relays receive the downlink RF signals transmitted by the source, which is divided into two portions by their own power splitters, i.e., one for energy harvesting and the other for information decoding;
- *Energy harvesting:* The portion of the received RF signal flowing to the energy harvesters is harvested and stored into the batteries of the relays' only energy source;
- *Information decoding:* The portion of the received signal flowing to the information decoder is decoded by consuming the harvested energy;

- *Information forwarding:* The relays forward the information from the source to the destination only if the information is decoded correctly.

The destination node is equipped with a single antenna for receiving the information signal from the relays and the source node.

Our downlink SWIPT-CCN adopts a classic time-division-multiple-access (TDMA) protocol in medium-access-contol (MAC) layer. A single transmission cycle consists of L TFs. A complete TF having a duration of T is composed of two equal time slots, which is characterised in Fig. 1 (b). During the first time slot, the source broadcasts the downlink RF signals to the relays and the destination. Specifically, since only one relay is activated for decoding and forwarding the information in a single frame, SWIPT from the source to the selected relay m ($m \in \{1, 2, \cdots, M\}$), WPT from the source to other relays and WIT from the source to the destination are carried out. The relay m then forwards the successfully decoded information during the second time slot.

B. Channel Aging Effect

The downlink WIT is completed via both the two-hop link and the direct link. Note that the two-hop transmission consists of the 1st-hop from the source to the relay m and the 2nd-hop from the relay m to the destination, as shown in Fig. 1 (a).

Channel aging effect is considered in this paper [18]. The small-scale fading coefficients of channels under the channel aging effect are formulated as

$$\begin{aligned}\mathbf{H}(l) &= \lambda_{s,m}\mathbf{H}(l-1) + \Delta\mathbf{H}(l) \\ &= \lambda^{l-1}\mathbf{H}(1) + \sum_{l'=2}^{l}\lambda^{l-l'}\Delta\mathbf{H}(l'),\end{aligned} \tag{1}$$

for $\forall l = 2, 3, \cdots, L$. $\lambda \in [0, 1]$ represents the temporal correlation coefficient. $\Delta\mathbf{H}(l) \sim \mathcal{CN}(0, (1-\lambda^2)\sigma^2)$ is the independent innovation component during the l-th TF, where σ^2 is the channel variation coefficient [18]. Note that $\{\Delta\mathbf{H}(l)|\forall l = 2, \cdots, L\}$ are independent with one another. Furthermore, $\mathbf{H}(l)$ follows a distribution of $\mathcal{CN}(\lambda^{l-1}\mathbf{H}(1), \sum_{l'=2}^{l}\lambda^{2(l-l')}(1-\lambda^2)\sigma^2)$.

Note that the matrix size of $\mathbf{H}(l)$ and $\Delta\mathbf{H}(l)$ depends on the channel dimension, i.e., the number of antennas of the transmitter and the receiver. Specifically, the normalised fading coefficients of the downlink channel from the source's N_s transmit antennas to the relay m's N_r antennas (the 1st-hop), that from the relay m's N_r antennas to the destination (the 2nd-hop) and that from the source's N_s antennas to the destination (the direct link) during the l-th TF are denoted as a $N_r \times N_s$ matrix $\mathbf{H}_{s,m}(l)$, a $1\times N_r$ $\mathbf{h}_{m,d}(l)$ and a $1\times N_s$ $\mathbf{h}_{s,d}(l)$, respectively. Therefore, the corresponding independent innovation components of the three channels are denoted as a $N_r \times N_s$ matrix $\Delta\mathbf{H}_{s,m}(l)$, a $1 \times N_r$ $\Delta\mathbf{h}_{m,d}(l)$ and a $1 \times N_s$ $\Delta\mathbf{h}_{s,d}(l)$. The corresponding temporal correlation coefficients and the channel variation coefficients are represented as $\{\lambda_{s,m}, \lambda_{m,d}, \lambda_{s,d}\}$ and $\{\sigma^2_{s,m}, \sigma^2_{m,d}, \sigma^2_{s,d}\}$.

Moreover, $\Omega_{s,m}$, $\Omega_{m,d}$ and $\Omega_{s,d}$ represent the large-scale path-loss between the source and the relay m, that between the relay m and the destination and that between the source and the destination, respectively.

III. Problem Formulation

A. SWIPT in the 1st-Hop Transmission

The source broadcasts a modulated RF signal $x(l) \sim \mathcal{CN}(0, 1)$ during the 1st-slot of the l-th TF. The received RF signal at the relay m is expressed as Eq. (2) for $\forall m = 1, \cdots, M$, where $P_s(l)$ is the transmit power of the source. Moreover, $\mathbf{w}_s(l)$ is a $N_s \times 1$ normalised transmit beamformer satisfying $\mathrm{Tr}\left(\mathbf{w}_s(l)\mathbf{w}_s^\dagger(l)\right) \leq 1$. The $N_r \times 1$ vector $\mathbf{n}_m(l) \sim \mathcal{CN}(0, \sigma_m^2\mathbf{I}_{N_r})$ represents the additive noise.

After adopting a maximal ratio combiner (MRC) $\mathbf{w}_{c,m} = \frac{\mathbf{H}_{s,m}(1)\mathbf{w}_s(l)}{\|\mathbf{H}_{s,m}(1)\mathbf{w}_s(l)\|}$ at the relay m, the power of the combined signal $\mathbf{w}_{c,m}\mathbf{y}_m(l)$ is formulated as

$$\begin{aligned}P_{\mathrm{c,m}}(l) = \lambda_{s,m}^{2(l-1)}\frac{P_s(l)}{\Omega_{s,m}}\mathrm{Tr}\left(\mathbf{H}_{s,m}(1)\mathbf{w}_s(l)\mathbf{w}_s^\dagger(l)\mathbf{H}_{s,m}^\dagger(1)\right) \\ + \left(1-\lambda_{s,m}^{2(l-1)}\right)\frac{P_s(l)}{\Omega_{s,m}}\sigma_{s,m}^2 + \sigma_m^2.\end{aligned} \tag{3}$$

A vector of power splitting factors is defined as $\boldsymbol{\rho}_m = \{\rho_m(l)|l = 1, \cdots, L\}$, where $\rho_m(l) \in [0, 1]$ represents the relay m's power-splitting factor during the l-th TF. Specifically, a fraction $\sqrt{1-\rho_m(l)}$ of the combined RF signal $\mathbf{w}_{c,m}\mathbf{y}_m(l)$ is exploited for the information decoding. Therefore, by considering the independent innovation component $\Delta\mathbf{H}_{s,m}(l)$ as the measurement error and following the corresponding derivation in Eq. (46) of [28], the lower-bound signal-to-noise-ratio (SNR) of the signal $\sqrt{1-\rho_m(l)}\mathbf{w}_{c,m}\mathbf{y}_m(l)$ with imperfect CSI is formulated as Eq. (4), where σ^2_{cov} is the power of the

$$\mathbf{y}_m(l) = \begin{cases}\sqrt{P_s(l)/\Omega_{s,m}}\mathbf{H}_{s,m}(l)\mathbf{w}_s(l)x(l) + \mathbf{n}_m(l), & \text{for } l = 1, \\ \sqrt{P_s(l)/\Omega_{s,m}}\left(\lambda_{s,m}^{l-1}\mathbf{H}_{s,m}(1) + \sum_{l'=2}^{l}\lambda_{s,m}^{l-l'}\Delta\mathbf{H}_{s,m}(l')\right)\mathbf{w}_s(l)x(l) + \mathbf{n}_m(l), & \text{for } \forall l = 2, \cdots, L\end{cases} \tag{2}$$

$$\gamma_m(l) = \frac{(1-\rho_m(l))\lambda_{s,m}^{2(l-1)}P_s(l)\mathrm{Tr}\left(\mathbf{H}_{s,m}(1)\mathbf{w}_s(l)\mathbf{w}_s^\dagger(l)\mathbf{H}_{s,m}^\dagger(1)\right)}{(1-\rho_m(l))\left(1-\lambda_{s,m}^{2(l-1)}\right)P_s(l)\sigma_{s,m}^2 + \Omega_{s,m}\left[(1-\rho_m(l))\,\sigma_m^2 + \sigma_{cov}^2\right]} \tag{4}$$

$$y_{s,d}(l) = \begin{cases} \sqrt{P_s(l)/\Omega_{s,d}}\mathbf{h}_{s,d}(l)\mathbf{w}_s(l)x(l) + n_d(l), & \text{for } l = 1, \\ \sqrt{P_s(l)/\Omega_{s,d}}\left(\lambda_{s,d}^{l-1}\mathbf{h}_{s,d}(1) + \sum_{l'=2}^{l}\lambda_{s,d}^{l-l'}\Delta\mathbf{h}_{s,d}(l')\right)\mathbf{w}_s(l)x(l) + n_d(l), & \text{for } \forall l = 2, \cdots, L. \end{cases} \tag{12}$$

Gaussian distributed noise incurred by the imperfect passband-to-baseband converter.

The information rate of the relay m during the l-th TF is expressed as $r_m(l) = \log(1 + \gamma_m(l))$ bps/Hz. The corresponding information decoding power is formulated as [14]

$$\varphi_m(l) = f_{dc}\left(2^{r_m(l)} - 1\right), \tag{5}$$

where f_{dc} represents the decoding cost factor.

Moreover, the other portion of the combined signal for the energy harvesting is $\sqrt{\rho_m(l)}\mathbf{w}_{c,m}\mathbf{y}_m(l)$. Therefore, the power harvested by a practical non-linear energy harvester of the relay m during the l-th TF is formulated as

$$P_{he,m}(l) = \frac{\psi - P_{sat}\Theta}{1 - \Theta}, \tag{6}$$

where we have $\Theta = \frac{1}{1+e^{ab}}$ and $\psi = \frac{P_{sat}}{1+e^{-a(\rho_m(l)P_{c,m}(l)-b)}}$. The parameters P_{sat}, a and b are determined by the circuitry of the energy harvester [29]. Therefore, the energy harvested is $E_m(l) = \frac{T}{2}P_{he,m}(l)$.

Since only a single designated relay is activated for decoding and forwarding during a single transmission cycle, the activation pattern of relays can be represented by a binary indicator vector $\boldsymbol{\alpha} = \{\alpha_m | m = 1, \cdots, M\}$ obeying the following constraints:

$$\sum_{m=1}^{M}\alpha_m \leq 1, \tag{7}$$

$$\alpha_m \in \{0, 1\}, \forall m = 1, \cdots, M. \tag{8}$$

Note that $\alpha_m = 1$ represents relay m is activated, otherwise, $\alpha_m = 0$. Furthermore, we consider that the relays can only decode information correctly, when the SNR $\gamma_m(l)$ for the information decoding is higher than a threshold $\gamma_{m,th}$, namely $\gamma_m(l) \geq \gamma_{m,th}$. The corresponding boolean results are expressed as $\boldsymbol{\beta}_m = \{\beta_m(l) | l = 1, \cdots, L\}$, for $\forall m = 1, \cdots, M$, where $\beta_m(l) = 1$ represents that the relay m decodes information correctly during the l-th TF, otherwise, $\beta_m(l) = 0$. The residual energy $Q_m(l)$ of the relay m at the end of the l-th TF is formulated as

$$Q_m(l) = Q_m(l-1) + E_{cur,m}(l), \tag{9}$$

where we define the energy $E_{cur,m}(l) \triangleq E_m(l) - \frac{T}{2}\alpha_m\left[\varphi_m(l) + \beta_m(l)P_m(l)\right]$ which characterises the difference between harvested energy and total consumption energy within the l-th TF. $Q_m(0)$ denotes the initial residual energy at the beginning of the current transmission cycle. The transmit power of the relay m is denoted as $\mathbf{P}_m = \{P_m(l) | l = 1, \cdots, L\}$.

B. WIT in the 2nd-Hop Transmission

The destination receives the RF signal transmitted by the relay m, which is expressed as

$$y_{m,d}(l) = \sqrt{\frac{P_m(l)}{\Omega_{m,d}}}\mathbf{h}_{m,d}(l)\mathbf{w}_m(l)x_m(l) + n_d(l), \tag{10}$$

for $\forall l = 1, \cdots, L$, where $x_m(l) \sim \mathcal{CN}(0, 1)$ is the modulated RF signal and $n_d(l) \sim \mathcal{CN}(0, \sigma_d^2)$ is the additive noise. Note that $\mathbf{w}_m(l)$ represents the transmit beamformer of the relay m, which can be formulated as $\mathbf{w}_m(l) = \mathbf{h}_{m,d}^{\dagger}(l)/\parallel \mathbf{h}_{m,d}(l) \parallel$ by adopting the optimal maximum-ratio-transmission (MRT) method in multiple-input-single-output (MISO) systems [30]. Similar to Eq. (4), the SNR of $y_{m,d}(l)$ is formulated as

$$\gamma_{m,d}(l) = \frac{\lambda_{m,d}^{2(l-1)}P_m(l) \parallel \mathbf{h}_{m,d}(1) \parallel^2}{\left(1 - \lambda_{m,d}^{2(l-1)}\right)\sigma_{m,d}^2 P_m(l) + \Omega_{m,d}\sigma_d^2}. \tag{11}$$

C. WIT in Direct Link

In the direct link, the RF signal $y_{s,d}(l)$ received by the destination is expressed as Eq. (12).

Similar to Eq. (4), the SNR of $y_{s,d}(l)$ is formulated as

$$\gamma_{s,d}(l) = \frac{\lambda_{s,d}^{2(l-1)}P_s(l)\mathrm{Tr}(\mathbf{h}_{s,d}(1)\mathbf{w}_s(l)\mathbf{w}_s^{\dagger}(l)\mathbf{h}_{s,d}^{\dagger}(1))}{\left(1 - \lambda_{s,d}^{2(l-1)}\right)P_s(l)\sigma_{s,d}^2 + \Omega_{s,d}\sigma_d^2}. \tag{13}$$

During the l-th TF, the destination receives RF signals from the source and the relay m successively, namely $y_{m,d}(l)$ and $y_{s,d}(l)$. After combining the two signals by the maximum ratio merging [31], the e2e throughput from the source to the destination can be formulated as

$$R(l) = \frac{T}{2}\log(1 + \sum_{m=1}^{M}\alpha_m\beta_m(l)\gamma_{m,d}(l) + \gamma_{s,d}(l)). \tag{14}$$

D. Downlink Sum-Throughput Maximisation

Our joint resource scheduling design can be formulated as:

$$\text{(P1)}: \max_{\mathbf{w}_s(l), \boldsymbol{\rho}_m, \mathbf{P}_m, \boldsymbol{\alpha}} R_{e2e} = \sum_{l=1}^{L}R(l), \tag{15}$$

$$\text{s. t. } \mathrm{Tr}\left(\mathbf{w}_s(l)\mathbf{w}_s^{\dagger}(l)\right) \leq 1, \forall l = 1, \cdots, L, \tag{15a}$$

$$0 \leq \rho_m(l) \leq 1, \forall m = 1, \cdots, M, \forall l = 1, \cdots, L, \tag{15b}$$

$$P_m(l) \geq 0, \forall m = 1, \cdots, M, \forall l = 1, \cdots, L, \tag{15c}$$

$$Q_m(l) \geq 0, \forall m = 1, \cdots, M, \forall l = 1, \cdots, L, \tag{15d}$$

$$\sum_{m=1}^{M}\alpha_m\beta_m(l)\gamma_m(l) \geq \sum_{m=1}^{M}\alpha_m\beta_m(l)\gamma_{m,d}(l), \forall l = 1, \cdots, L, \tag{15e}$$

(7) and (8).

(P1) aims for maximising the downlink e2e sum-throughput during a single transmission cycle having L TFs in it by optimising the source's transmit beamformer $\mathbf{w}_s(l), \forall l = 1, \cdots, L$ in the spatial-domain, the relays' signal splitter $\boldsymbol{\rho}_m$ and transmit power $\mathbf{P}_m$ in the power-domain as well as the relays' binary activation indicator vector $\boldsymbol{\alpha}$ in the user-domain. Constraint (15a) ensures a normalised $\mathbf{w}_s(l)$. Constraints (15b)-(15d) limit the range of the relays' signal splitter, transmit power and residual energy, respectively. (15e) ensures data causality that the throughput in the 1st-hop transmission is not lower than that in the 2nd-hop. Furthermore, constraints (7) and (8) have been defined in Section III-A.

IV. Iterative Algorithm Aided Joint Design

Due to the coupled optimisation variables $\{\mathbf{w}_s(l), \boldsymbol{\rho}_m, \mathbf{P}_m\}$ as well as the discrete vector $\boldsymbol{\alpha}$, (P1) is non-convex. In this section, we firstly transform (P1) into a sub-problem (P2) by fixing the relays' activation vector $\boldsymbol{\alpha}$ as well as the decoding indicator vector $\boldsymbol{\beta}_m$. The local optimal solution to (P2) is then obtained by decoupling it into two sub-problems, which alternatively optimise the transmit beamformer $\mathbf{w}_s(l)$ of the source node as well as the power splitter $\boldsymbol{\rho}_m$ and the transmit power $\mathbf{P}_m$ of the activated relay, respectively, by fixing other optimisation variables. Finally, the joint design is obtained by searching $\boldsymbol{\alpha}$ and $\boldsymbol{\beta}_m$.

Let us assume that relay $m^\ddagger$ is activated, i.e., $\alpha_{m^\ddagger} = 1$, with fixed $\boldsymbol{\beta}_{m^\ddagger}$. A pair of non-overlapping sets $\mathcal{L}^+_{m^\ddagger,k}$ and $\mathcal{L}^-_{m^\ddagger,k}$ are defined as the indices of the TFs. We have $\beta_{m^\ddagger}(l) = 1$, i.e., $\gamma_{m^\ddagger}(l) \geq \gamma_{m^\ddagger,th}$ for $\forall l \in \mathcal{L}^+_{m^\ddagger,k}$, while $\beta_{m^\ddagger}(l) = 0$ indicates $\gamma_{m^\ddagger}(l) < \gamma_{m^\ddagger,th}$ for $\forall l \in \mathcal{L}^-_{m^\ddagger,k}$. Therefore, (P1) can be reformulated as

$$\text{(P2)}: \max_{\mathbf{w}_s(l), \boldsymbol{\rho}_{m^\ddagger}, \mathbf{P}_{m^\ddagger}} R_{e2e}, \tag{16}$$

$$\text{s. t. } \gamma_{m^\ddagger}(l) \geq \gamma_{m^\ddagger,th}, \forall l \in \mathcal{L}^+_{m^\ddagger,k}, \tag{16a}$$

$$\gamma_{m^\ddagger}(l) < \gamma_{m^\ddagger,th}, \forall l \in \mathcal{L}^-_{m^\ddagger,k}, \tag{16b}$$

$$\gamma_{m^\ddagger}(l) \geq \gamma_{m^\ddagger,d}(l), \forall l \in \mathcal{L}^+_{m^\ddagger,k}, \tag{16c}$$

$$\text{(15a), (15b), (15c) and (15d).}$$

Note that (P2) has no solution if the fixed $\boldsymbol{\beta}_{m^\ddagger}$ violates the constraints (16b) and (16c).

A. Transmit Beamforming Design $\mathbf{W}_s(l)$ of Source

When fixed $\{\boldsymbol{\rho}_{m^\ddagger}, \mathbf{P}_{m^\ddagger}\}$ is given, by letting $\mathbf{W}_s(l) = \mathbf{w}_s(l)\mathbf{w}_s^\dagger(l)$ as well as by relaxing the rank-one constraint on the positive semi-definite covariance matrix $\mathbf{W}_s(l)$, (P2) can be reformulated as the following covariance matrix design in the spatial-domain:

$$\text{(P2-1)}: \max_{\mathbf{W}_s(l)} R_{e2e} \tag{17}$$

$$\text{s. t. (15a), (15d), (16a), (16b), and (16c).}$$

Since the constraint (15d) is non-convex, (P2-1) is a non-convex problem. Nevertheless, given the fixed $\mathbf{W}_s(l)$, for $l \neq l^\ddagger$ and $\forall l, \forall l^\ddagger = 1, \cdots, L$, the source's transmit beamforming $\mathbf{W}_s(l^\ddagger)$ during the time-slot $l^\ddagger$ can be optimised by equivalently transforming the constraint (15d) to an affine constraint. Specifically, the constraint (15d) can be rewritten as

$$Q_{m^\ddagger}(l^\ddagger - 1) + \sum_{l'=l^\ddagger}^{l} E_{cur,m^\ddagger}(l') \geq 0, \ \forall l = l^\ddagger, \cdots, L, \tag{18}$$

where we have $E_{cur,m^\ddagger}(l) = E_{m^\ddagger}(l) - \frac{T}{2}\alpha_{m^\ddagger}\left[\varphi_{m^\ddagger}(l) + \beta_{m^\ddagger}(l)P_{m^\ddagger}(l)\right]$, according to Eq. (9). Observe from Eq. (18) that $E_{cur,m^\ddagger}(l^\ddagger)$ is a function with respect to $\mathbf{W}_s(l^\ddagger)$, while $Q_c \triangleq Q_{m^\ddagger}(l^\ddagger - 1) + \sum_{l'=l^\ddagger+1}^{l} E_{cur,m^\ddagger}(l')$ is a constant by fixing $\mathbf{W}_s(l)$, $l \neq l^\ddagger$. Therefore, The constraint (15d) can be further rewritten as

$$Q_c + E_{m^\ddagger}(l^\ddagger) - \frac{T}{2}\alpha_{m^\ddagger}\left[\varphi_{m^\ddagger}(l^\ddagger) + \beta_{m^\ddagger}(l^\ddagger)P_{m^\ddagger}(l^\ddagger)\right] \geq 0. \tag{19}$$

Unfortunately, it is still a non-convex constraint. Hence, *Lemma 1* is proposed to simplify it into an affine constraint. We define $W \triangleq \mathrm{Tr}\left(\mathbf{H}_{s,m^\ddagger}(1)\mathbf{W}_s(l^\ddagger)\mathbf{H}^\dagger_{s,m^\ddagger}(1)\right)$ for $W \geq 0$. The left-hand-side of the constraint (19) is denoted by a function $\Gamma(W)$ with respect to W.

Lemma 1: The constraint (19) can be equivalently transformed into Eq. (20) on the next page, where we have $\kappa_1 = \frac{f_{dc}P_sTP_{sat}\rho_{m^\ddagger}(l)\lambda^{2(l-1)}_{s,m^\ddagger}(1+e^{ab})}{2\Omega_{s,m^\ddagger}e^{ab}}$ and $\kappa_2 = \frac{2f_{dc}P_sT(1-\rho_{m^\ddagger}(l))\lambda^{2(l-1)}_{s,m^\ddagger}}{(1-\rho_{m^\ddagger}(l))\left(1-\lambda^{2(l-1)}_{s,m^\ddagger}\right)P_s\sigma^2_{s,m^\ddagger}+\Omega_{s,m^\ddagger}\left[\left(1-\rho_{m^\ddagger}(l)\right)\sigma^2_{m^\ddagger}+\sigma^2_{cov}\right]}$. Moreover, $[W]^{W_{up}}_{W_{low}}$ denotes the range of W in three different cases A-C listed in Eq. (21) on the next page, where we have $\omega_i = \frac{(-\ln x_i + ab)\Omega_{s,m^\ddagger}}{a\rho_{m^\ddagger}(l)\lambda^{2(l-1)}_{s,m^\ddagger}P_s}$ for $\forall i = 1, 2$, $x_1 = -\frac{2\kappa_3+2\sqrt{\kappa_3^2-\kappa_2^2/4}}{\kappa_2}$, $x_2 = \frac{-2\kappa_3+2\sqrt{\kappa_3^2-\kappa_2^2/4}}{\kappa_2}$ and $\kappa_3 = \frac{\kappa_2}{2} - \kappa_1$. Specifically, cases A, B and C denote $e^{ab} \leq x_1 < x_2$, $0 < x_1 \leq e^{ab} \leq x_2$ and $0 < x_1 < x_2 < e^{ab}$, respectively. Moreover, $W_{k(i,j)}$ expressing the boundary of W, for $k \in \{1, 2\}$, $i \in \{0, \omega_1, \omega_2\}$ and $j \in \{\omega_1, \omega_2, \infty\}$ is obtained by the bisection method based algorithm, which is detailed in the pseudo code of Algorithm 1.

Proof: Please refer to Appendix A for the detailed proof. ■

Algorithm 1 has the following main steps:

- *Step 1*: Initialise the search range $[W_{min}, W_{max}]$ of the bisection method according to i and j, as shown in Line 1 of Algorithm 1.
- *Step 2*: Update the central point W_{mid} and obtain $\Gamma(W_{mid})$ by substituting $W \leftarrow W_{mid}$ into it. $k \in \{1, 2\}$ is the monotonicity indicator. $\Gamma(W)$ is monotonically increasing when we have $k = 1$, otherwise, it is decreasing. According to its different monotonicity, the corresponding bisection method is carried out. This step is characterised in Lines 3-9 of Algorithm 1.

$$\begin{cases} 0 \le W \le W_{2(0,\infty)}, & \text{if } \kappa_1(\kappa_1-\kappa_2) \le 0 \bigcap \Gamma(0) \ge 0 \\ \text{No solution}, & \text{if } \kappa_1(\kappa_1-\kappa_2) \le 0 \bigcap \Gamma(0) < 0 \\ [W]_{W_{low}}^{W_{up}}, & \text{otherwise} \end{cases} \tag{20}$$

$$[W]_{W_{low}}^{W_{up}} = \begin{cases} \begin{cases} 0 \le W \le W_{2(0,\infty)}, & \text{if } \Gamma(0) \ge 0, \\ \text{No solution}, & \text{if } \Gamma(0) < 0, \end{cases} & \text{for case A} \\ \begin{cases} 0 \le W \le W_{2(\omega_1,\infty)}, & \text{if } \Gamma(0) \ge 0 \bigcap \Gamma(\omega_1) > 0, \\ W_{1(0,\omega_1)} \le W \le W_{2(\omega_1,\infty)}, & \text{if } \Gamma(0) < 0 \bigcap \Gamma(\omega_1) \ge 0, \\ \text{No solution}, & \text{if } \Gamma(0) < 0 \bigcap \Gamma(\omega_1) < 0, \end{cases} & \text{for case B} \\ \begin{cases} \text{No solution}, & \text{if } \Gamma(0) \le 0 \bigcap \Gamma(\omega_1) < 0 \bigcap \Gamma(\omega_2) < 0, \\ W_{1(\omega_2,\omega_1)} \le W \le W_{2(\omega_1,\infty)}, & \text{if } \Gamma(0) \le 0 \bigcap \Gamma(\omega_1) \ge 0 \bigcap \Gamma(\omega_2) \le 0, \\ 0 \le W \le W_{2(0,\omega_2)}, & \text{if } \Gamma(0) > 0 \bigcap \Gamma(\omega_1) < 0 \bigcap \Gamma(\omega_2) < 0, \\ 0 \le W \le W_{2(0,\omega_2)} \bigcup & \\ W_{1(\omega_2,\omega_1)} \le W \le W_{2(\omega_1,\infty)}, & \text{if } \Gamma(0) > 0 \bigcap \Gamma(\omega_1) > 0 \bigcap \Gamma(\omega_2) < 0, \\ 0 \le W \le W_{2(\omega_1,\infty)}, & \text{if } \Gamma(0) > 0 \bigcap \Gamma(\omega_1) \ge 0 \bigcap \Gamma(\omega_2) \ge 0, \end{cases} & \text{for case C} \end{cases} \tag{21}$$

Algorithm 1 Bisection method based algorithm for searching $W_{k(i,j)}$

Input: The physical/MAC layer parameters, such as N_s, N_r, $\Omega_{s,m}$, $\lambda_{s,m}$, $\sigma_{s,m}^2$, σ_m^2, $m^\ddagger$ and $l^\ddagger$. Source's transmit beamformer $\mathbf{W}_s(l)$ for $l = 1, \cdots, L$ and $l = l^\ddagger$. Relay's signal splitter $\boldsymbol{\rho}_m$ and transmit power vector $\boldsymbol{P}_m$. The discrete vectors $\{\boldsymbol{\alpha}_m, \boldsymbol{\beta}_m\}$. k, i and j in $W_{k(i,j)}$. Difference threshold ς.
Output: Boundary $W_{k(i,j)}$ of W.
1: Initialise $W_{min} \leftarrow i$ and $W_{max} \leftarrow j$;
2: **while** $W_{max} - W_{min} \geq \varsigma$ **do**
3: Update $W_{mid} \leftarrow \frac{W_{min}+W_{max}}{2}$;
4: Obtain $\Gamma(W_{mid})$;
5: **if** $k = 1$ **then**
6: If $\Gamma(W_{mid}) > 0$, then $W_{max} \leftarrow W_{mid}$; otherwise, $W_{min} \leftarrow W_{mid}$;
7: **else**
8: If $\Gamma(W_{mid}) > 0$, then $W_{min} \leftarrow W_{mid}$; otherwise, $W_{max} \leftarrow W_{mid}$;
9: **end if**
10: **end while**
11: **return** $W_{k(i,j)} = W_{mid}$.

- *Step 3*: If the difference between W_{min} and W_{max} is higher than a pre-defined threshold ς, repeat Step 2. Otherwise, obtain $W_{k(i,j)} = W_{mid}$ as output, as shown in Lines 2 and 11 of Algorithm 1.

According to *Lemma 1*, given the fixed $\mathbf{W}_s(l)$, for $\forall l = 1, \cdots, L$ and $l \neq l^\ddagger$, (P2-1) can be equivalently reformulated as

$$\text{(P2-2)}: \max_{\mathbf{W}_s(l^\ddagger)} R_{e2e} \tag{22}$$
$$\text{s. t. (15a), (15d), (16a), (16b), (16c), (20) and (21).}$$

(P2-2) is a convex optimisation problem, which it can be solved by any convex optimisation tool, such as CVX.

Complexity analysis: The complexity of the interior point method based convex optimisation tool for solving the sub-problem (P2-2) is $O\left(\frac{N_s^2+N_s}{2}\right)^{3.5}$ [32]. The complexity of bi-section method in Algorithm 1 is $O\left(\log\left(\frac{j-i}{\varsigma}\right)\right)$. Therefore, the complexity for solving (P2-2) is $O\left(3\log\left(\frac{j-i}{\varsigma}\right) + \left(\frac{N_s^2+N_s}{2}\right)^{3.5}\right)$.

B. Transmit Power Design $\mathbf{P}_{m^\ddagger}$ and Power Splitter Design $\boldsymbol{\rho}_{m^\ddagger}$ of Relay $m^\ddagger$

Given fixed $\{\mathbf{W}_s(l)\}$, we have the optimal power splitter $\rho_{m^\ddagger}^*(l) = 1$ and the optimal transmit power $P_{m^\ddagger}^*(l) = 0$ for $\forall l \in \mathcal{L}_{m^\ddagger,k}^-$, since the relay fails to correctly decode the received information. Therefore, the whole signal from the source node is utilised for energy harvesting and the relay does not forward any information during the TF l. In the case of $\forall l \in \mathcal{L}_{m^\ddagger,k}^+$, the relay $m^\ddagger$ forwards the successfully decoded information to the destination node, i.e., $0 \le \rho_{m^\ddagger}^*(l) \le 1$ and $P_{m^\ddagger}^*(l) \ge 0$. As a result, (P2) can be reformulated as

$$\text{(P2-3)}: \max_{P_{m^\ddagger}(l), \rho_{m^\ddagger}(l), \forall l \in \mathcal{L}_{m^\ddagger,k}^+} R_{e2e} \tag{23}$$
$$\text{s. t. (15b), (15c), (15d), (16a), (16b), and (16c).}$$

Although (P2-3) is non-convex owing to the non-convex constraint (15d), we can obtain the optimal solution to (P2-3) by finding a fact for the residual energy $Q_{m^\ddagger}(l)$ of the relay $m^\ddagger$, which is detailed in *Lemmas 2-3* and *Theorem 1*.

Lemma 2: We have Eq. (24). Specifically, if the activated relay $m^\ddagger$ decodes information correctly during a single TF, it may deplete its residual energy to forward information.

$$Q_{m^\ddagger}(l) = 0, \forall l \in \mathcal{L}_{m^\ddagger,k}^+. \tag{24}$$

Proof: Please refer to Appendix B for detailed proof. ■

According to *Lemma 2*, we further have *Lemma 3* for $Q_{m^\ddagger}(l)$ in the constraint (15d).

Lemma 3: $Q_{m^\ddagger}(l-1)$ in Eq. (9) is a constant.

Proof: For $(l-1) \in \mathcal{L}_{m^\ddagger,k}^+$, we have $Q_{m^\ddagger}(l-1) = 0$ according to Eq. (24) in *Lemma 2*. Otherwise, we have $Q_{m^\ddagger}(l-1) = Q_{m^\ddagger}(l') + \sum_{\hat{l}=l'+1}^{l-1} E_{cur,m^\ddagger}(\hat{l})$ for $l' < l-1$, $l' \in \mathcal{L}_{m^\ddagger,k}^+$ and $\hat{l} \in \mathcal{L}_{m^\ddagger,k}^-$.

Algorithm 2 Bisection method based algorithm for searching $\rho_{m^\ddagger}(l)$ and $P_{m^\ddagger}(l)$

Input: The physical/MAC layer parameters, such as N_s, N_r, $\Omega_{s,m}$, $\lambda_{s,m}$, $\sigma^2_{s,m}$, σ^2_m, $m^\ddagger$. Source's transmit beamformer $\mathbf{W}_s(l)$ for $l = 1, \cdots, L$. Relay's signal splitter $\rho_{m^\ddagger}(l) = 1$ and transmit power $P_{m^\ddagger}(l) = 0$ for $\forall l \in \mathcal{L}^-_{m^\ddagger,k}$. The discrete vectors $\{\boldsymbol{\alpha}_m, \boldsymbol{\beta}_m\}$. Difference threshold ς.

Output: The optimal power splitter $\rho^*_{m^\ddagger}(l)$ and the optimal transmit power $P^*_{m^\ddagger}(l)$ for $\forall l \in \mathcal{L}^+_{m^\ddagger,k}$.

1: Initialise $\rho_{min}(l) \leftarrow 0$ and $\rho_{max}(l) \leftarrow 1$ for $\forall l \in \mathcal{L}^+_{m^\ddagger,k}$;
2: **while** $\rho_{max}(l) - \rho_{min}(l) \geq \varsigma$ **do**
3: Update $\rho_{m^\ddagger}(l) \leftarrow \frac{\rho_{max}(l)+\rho_{min}(l)}{2}$;
4: Update $P_{m^\ddagger}(l)$ by substituting $\rho_{m^\ddagger}(l)$ into Eq. (24);
5: Obtain $\gamma_{m^\ddagger}(l)$ and $\gamma_{m^\ddagger d}(l)$ by substituting $\rho_{m^\ddagger}(l)$ and $P_{m^\ddagger}(l)$ into Eq. (4) and Eq. (11), respectively;
6: **if** $\gamma_{m^\ddagger}(l) \geq \gamma_{m^\ddagger d}(l)$ **then**
7: $\rho_{min}(l) \leftarrow \rho_{m^\ddagger}(l)$;
8: **else**
9: $\rho_{max}(l) \leftarrow \rho_{m^\ddagger}(l)$;
10: **end if**
11: **end while**
12: **return** $\rho^*_{m^\ddagger}(l) = \rho_{min}(l)$ and $P^*_{m^\ddagger}(l)$ by substituting $\rho^*_{m^\ddagger}(l)$ into Eq. (24).

Note that $Q_{m^\ddagger}(l') = 0$. Moreover, we have $\rho^*_{m^\ddagger}(\hat{l}) = 1$ and $P^*_{m^\ddagger}(\hat{l}) = 0$, which results in a constant $E_{cur,m^\ddagger}(\hat{l})$. *Lemma 3* is proved. ∎

Theorem 1: The optimal power splitter $\rho^*_{m^\ddagger}(l)$ and the optimal transmit power $P^*_{m^\ddagger}(l)$ for $\forall l \in \mathcal{L}^+_{m^\ddagger,k}$ satisfy

$$\gamma_{m^\ddagger}(l) = \gamma_{m^\ddagger d}(l). \tag{25}$$

Proof: In the constraint (16c), $\gamma_{m^\ddagger}(l)$ is monotonously decreasing as we increase $\rho_{m^\ddagger}(l)$, while $\gamma_{m^\ddagger d}(l)$ is a monotonously increasing function with respect to $P_{m^\ddagger}(l)$. Moreover, according to *Lemmas 2* and *3*, given a fixed $\rho_{m^\ddagger}(l)$, the corresponding transmit power $P_{m^\ddagger}(l)$ can be obtained by Eq. (24), while $P_{m^\ddagger}(l)$ has positive correlation with $\rho_{m^\ddagger}(l)$. Therefore, $\gamma_{m^\ddagger d}(l)$ increases as we increase $\rho_{m^\ddagger}(l)$. Observe from (P2-3) that its objective function is monotonously increasing as we increase $P_{m^\ddagger}(l)$. Therefore, the objective has positive correlation with $\rho_{m^\ddagger}(l)$. As a result, a power splitter $\rho^*_{m^\ddagger}(l)$ and the corresponding transmit power $P^*_{m^\ddagger}(l)$ following Eq. (25) can obtain a maximum e2e throughput R^*_{e2e}, which are the optimal solution to (P2-3). *Theorem 1* is proved. ∎

Since $\gamma_{m^\ddagger}(l)$ is monotonously decreasing and $\gamma_{m^\ddagger d}(l)$ is monotonously increasing as we increase $\rho_{m^\ddagger}(l)$. A bisection method based algorithm is developed to obtain the power splitter $\rho^*_{m^\ddagger}(l)$ and the corresponding transmit power $P^*_{m^\ddagger}(l)$ satisfying Eq. (25), for $\forall l \in \mathcal{L}^+_{m^\ddagger,k}$ in (P2-3). Its pseudo code is provided in Algorithm 2, which has the following steps:

- *Step 1*: Initialise the search range $[\rho_{min}(l), \rho_{max}(l)]$ of the bisection method, as shown in Line 1 of Algorithm 2.
- *Step 2*: Update $\rho_{m^\ddagger}(l)$ as the center point of the range $[\rho_{min}(l), \rho_{max}(l)]$, while calculating the corresponding $P_{m^\ddagger}(l)$ by Eq. (24). The SNR $\gamma_{m^\ddagger}(l)$ for the information decoding at relay $m^\ddagger$ and that $\gamma_{m^\ddagger d}(l)$ at the destination node can be updated by Eq. (4) and Eq. (11), respectively. Note that there is a negative correlation between $\gamma_{m^\ddagger}(l)$ and $\rho_{m^\ddagger}(l)$. Therefore, $\rho_{m^\ddagger}(l)$ can be increased when we have $\gamma_{m^\ddagger}(l) \geq \gamma_{m^\ddagger d}(l)$. Therefore, update $\rho_{min}(l) \leftarrow \rho_{m^\ddagger}(l)$. Otherwise, we decrease $\rho_{m^\ddagger}(l)$ to satisfy the constraint (16c). This step is characterised in Lines 3-10 of Algorithm 2.
- *Step 3*: If the difference of the search range is higher than the difference threshold ς, repeat Step 2, as shown in Line 2 of Algorithm 2. Otherwise, obtain the power splitter $\rho^*_{m^\ddagger}(l)$ and the transmit power $P^*_{m^\ddagger}(l)$ for $\forall l \in \mathcal{L}^+_{m^\ddagger,k}$, as shown in Line 12 of Algorithm 2.

Performance analysis: The optimal solution to (P2-3) can be obtained when the difference threshold $\varsigma \to 0$. Let us consider a power splitter $\rho'_{m^\ddagger}(l)$ satisfying $0 \leq \rho'_{m^\ddagger}(l) < \rho^*_{m^\ddagger}(l)$. According to the proof of *Theorem 1*, although the constraint (16c) can be satisfied, the obtained e2e throughput R'_{e2e} is lower than R^*_{e2e}. Moreover, when we have $1 \geq \rho'_{m^\ddagger}(l) > \rho^*_{m^\ddagger}(l)$, $\rho'_{m^\ddagger}(l)$ is not a feasible solution to (P2-3) since the constraint (16c) cannot be satisfied. Therefore, $\rho^*_{m^\ddagger}(l)$ and the corresponding $P^*_{m^\ddagger}(l)$ can obtain a maximum e2e throughput R^*_{e2e}.

Complexity analysis: The complexity of bisection method aided Algorithm 2 is $O\left(\log\left(\frac{1}{\varsigma}\right)\right)$.

C. Relay selection Design $\boldsymbol{\alpha}$

We consider a partial relay selection (PRS) scheme, in which the relay has the highest SNR in the 1st-hop is selected as a forwarder. It is formulated as

$$m^\ddagger = \arg \max_{m=1,\cdots,M} \gamma_m(1), \tag{26}$$

where $m^\ddagger$ denotes the selected relay and $\gamma_m(1)$ expresses the SNR of the relay m's received signal for information decoding during the first TF. PRS is a classical strategy in relaying networks due to its low complexity [33].

D. Joint Design

Given the local optimal solution obtained from (P2), we may exploit PRS strategy for the relay selection, while traversing all possible binary indicator vector $\boldsymbol{\beta}_m$. However, the exhaustive search for $\boldsymbol{\beta}_m$ has a high complexity. Therefore, we exclude several TFs, when the selected relay cannot successfully decode the received information. The pseudo code of the proposed iterative joint design is detailed in Algorithm 3, which has the following main steps:

- *Step 1: Relay Selection.* Initialise power splitter $\rho_m(1)$ as zero and transmit power $P_m(1)$ as 5×10^{-3} W, for $\forall m = 1, \cdots, M$. Select a relay $m^\ddagger$ as the forwarder in the 2nd-hop transmission by substituting $\rho_m(1)$ into Eq. (26), as shown in Lines 1-2 of Algorithm 3.
- *Step 2: Forwarding Frame Selection.* In this step, before traversing the vector $\boldsymbol{\beta}_m$, a maximum SNR $\gamma_{m^\ddagger}(l)$ obtained by the relay $m^\ddagger$ is compared with the SNR threshold $\gamma_{m^\ddagger,th}$ to exclude a part of frames with failed decoding.

Algorithm 3 An iterative algorithm based joint design for solving (P1)

Input: All the phusical/MAC layer parameters, such as M, N_s, N_r, $\Omega_{s,m}$, $\Omega_{m,d}$, L, $\{(\mathbf{H}_{s,m}(l), \mathbf{h}_{m,d}(l), \mathbf{h}_{s,d}(l))|l = 1, \cdots, L\}$, $\gamma_{m,th}$, $\sigma^2_{s,m}$, $\sigma^2_{m,d}$ and $\sigma^2_{s,d}$. Difference threshold ς.
Output: Solution $\{\mathbf{W}^*_s(l), \mathbf{P}^*_m, \boldsymbol{\rho}^*_m, \boldsymbol{\alpha}^*\}$. E2e throughput R^*_{e2e}.
1: Initialise the power splitter $\rho_m(1) \leftarrow 0$ and transmit power $P_m(1) \leftarrow 5 \times 10^{-3}$W.
2: Select the relay $m^\ddagger$ by Eq. (26) and obtain $\boldsymbol{\alpha}^* \leftarrow \{\alpha_{m=m^\ddagger} \leftarrow 1, \alpha_{m\neq m^\ddagger} \leftarrow 0 | m = 1, \cdots, M\}$.
3: Obtain $\overline{\mathbf{W}}_s(l) \leftarrow \arg\max_{\mathbf{W}_s(l)} \mathrm{Tr}\left(\mathbf{H}_{s,m^\ddagger}(1)\mathbf{W}_s(l)\mathbf{H}^\dagger_{s,m^\ddagger}(1)\right)$, where $\mathbf{W}_s(l)$ satisfies (15a).
4: Obtain $\gamma_{m^\ddagger}(l)$ by substituting $\overline{\mathbf{W}}_s(l)$ and $\rho_{m^\ddagger}(l) \leftarrow 0$ into Eq. (4);
5: Obtain $\mathcal{L}^- = \{l | \gamma_{m^\ddagger}(l) < \gamma_{m^\ddagger,th}\}$ and initialise $k \leftarrow 0$.
6: **while** $k \leq 2^L - 1$ **do**
7: Update $\boldsymbol{\beta}_{m^\ddagger} \leftarrow \mathrm{binary}(k)$;
8: **if** $\beta_{m^\ddagger}(l) = 1$, for $l \in \mathcal{L}^-$ **then**
9: Continue;
10: **else**
11: Initialise $\mathbf{W}_{s,(0)}(l) \leftarrow \overline{\mathbf{W}}_s(l)$, $R_{e2e,cur} \leftarrow 0$, $R_{e2e,pre} \leftarrow -2\varsigma$ and iteration number $i \leftarrow 0$;
12: **while** $|R_{e2e,cur} - R_{e2e,pre}| > \varsigma$ **do**
13: $R_{e2e,pre} \leftarrow R_{e2e,cur}$;
14: Update $\boldsymbol{\rho}_{m^\ddagger,(i+1)} \leftarrow \boldsymbol{\rho}^*_{m^\ddagger}$ and $\mathbf{P}_{m^\ddagger,(i+1)} \leftarrow \mathbf{P}^*_{m^\ddagger}$ by carrying out Algorithm 2 with input of $\{\mathbf{W}_{s,(i)}(l)\}$;
15: Update $\mathbf{W}_{s,(i+1)}(l) \leftarrow \mathbf{W}^*_s(l)$, for $\forall l = 1, \cdots, L$ and $R_{e2e,cur}$ by solving (P2-2) after substituting $\{\boldsymbol{\rho}_{m^\ddagger,(i+1)}, \mathbf{P}_{m^\ddagger,(i+1)}\}$ into it;
16: Update $i \leftarrow i + 1$;
17: **end while**
18: Update $\{\mathbf{W'}_{s,k}(l), \boldsymbol{\rho'}_{m^\ddagger,k}, \mathbf{P'}_{m^\ddagger,k}\} \leftarrow \{\mathbf{W}_{s,(i)}(l), \boldsymbol{\rho}_{m^\ddagger,(i)}, \mathbf{P}_{m^\ddagger,(i)}\}$, $R_{e2e,k} \leftarrow R_{e2e,cur}$ and $k \leftarrow k + 1$;
19: **end if**
20: **end while**
21: Obtain $k^* \leftarrow \arg\max_k R_{e2e,k}$;
22: **return** $\boldsymbol{\alpha}^*$, $\{\mathbf{W}^*_s(l), \boldsymbol{\rho}^*_m, \mathbf{P}^*_m\} \leftarrow \{\mathbf{W'}_{s,k^*}(l), \boldsymbol{\rho'}_{m^\ddagger,k^*}, \mathbf{P'}_{m^\ddagger,k^*}\}$ and $R^*_{e2e} \leftarrow R_{e2e,k^*}$.

  - *Step 2-1*: Obtain the transmit beamformer $\overline{\mathbf{W}}_s(l)$ of the source node[1], which makes the relay $m^\ddagger$ obtain a maximum SNR $\gamma_{m^\ddagger}(l)$ by substituting it and $\rho_{m^\ddagger}(l) \leftarrow 0$ into Eq. (4). Define a set $\mathcal{L}^-$ to include the TFs with failed decoding and initialise the traversing number k to 0, as shown in Lines 3-5 of Algorithm 3.
  - *Step 2-2*: Traverse $\boldsymbol{\beta}_{m^\ddagger}$, as shown in Line 6 of Algorithm 3. For each $k \leq 2^L - 1$, if $\beta_{m^\ddagger}(l)$ for $l \in \mathcal{L}^-$ is set to 1, the constraint (16a) of (P2) cannot be satisfied. Therefore, skip Step 3, update $k \leftarrow k+1$ and repeat this substep. Otherwise, carry out Step 3, as shown in Lines 7-9 of Algorithm 3. When $k > 2^L - 1$, i.e., the traversal operation is completed, skip to Step 4.

- *Step 3: Transmit Power and Power Splitter Design for the Relay $m^\ddagger$.* Initialise the transmit beamforming matrix $\mathbf{W}_{s,(0)}(l)$ as $\overline{\mathbf{W}}_s(l)$. Initialise the e2e throughput $R_{e2e,cur}$ obtained in the current iteration, that $R_{e2e,pre}$ obtained in the last one and the iteration number i, as shown in Line 11 of Algorithm 3..
  - *Step 3-1*: By exploiting the optimal solution $\{\mathbf{W}_{s,(i)}(l), \boldsymbol{\rho}_{m^\ddagger,(i)}, \mathbf{P}_{m^\ddagger,(i)}\}$ obtained in the last iteration, we can sequentially update them as $\{\mathbf{W}_{s,(i+1)}(l), \boldsymbol{\rho}_{m^\ddagger,(i+1)}, \mathbf{P}_{m^\ddagger,(i+1)}\}$ by solving (P2-2) with any convex optimisation tool and (P2-3) with Algorithm 2, respectively, as characterised in Lines 13-16 of Algorithm 3.
  - *Step 3-2*: If the difference between $R_{e2e,cur}$ and $R_{e2e,pre}$ is higher than a pre-defined threshold ς, we start another iteration by repeating Step 3-1, as shown in Line 12 of Algorithm 3. Otherwise, obtain $\{\mathbf{W'}_{s,k}(l), \boldsymbol{\rho'}_{m^\ddagger,k}, \mathbf{P'}_{m^\ddagger,k}\} \leftarrow \{\mathbf{W}_{s,(i)}(l), \boldsymbol{\rho}_{m^\ddagger,(i)}, \mathbf{P}_{m^\ddagger,(i)}\}$ and $R_{e2e,k} \leftarrow R_{e2e,cur}$ as the solution and the throughput with different k.
- *Step 4: Output.* By obtaining k^* with the maximum $R_{e2e,k}$, $\{\mathbf{W'}_{s,k^*}(l), \boldsymbol{\rho'}_{m^\ddagger,k^*}, \mathbf{P'}_{m^\ddagger,k^*}, \boldsymbol{\alpha}^*\}$ and the corresponding R_{e2e,k^*} are output, as shown in Lines 21 and 22 of Algorithm 3.

Rank-1 recovery: Since a rank-1 relaxation is applied to (P2-1), the rank-1 solution need to be recovered after the convergence of Algorithm 3. The vector $\mathbf{w}^*_s(l)$ can be approximated by Gaussian randomisation methodology [34].

V. Numerical Results

We model the two-hop channels, namely, from the source to the relays and from the relays to the destination, as Rician fading channels, which can be formulated as $\mathbf{H}(1) = \sqrt{\frac{K_r}{K_r+1}}\mathbf{H}_0 + \sqrt{\frac{1}{K_r+1}}\mathbf{H}_\omega(1)$ [35]. K_r is the Rician factor, and $\mathbf{H}_\omega(1)$ is the channel matrix with entries following the Rayleigh distribution, while $\mathbf{H}_0$ is a deterministic matrix satisfying $\|\mathbf{H}_0\|^2 = N_r N_s$ and N_r for the 1st- and 2nd-hop channels, respectively. Moreover, we consider the Rayleigh fading for the direct link between the source and the destination, due to the blockage. The path-loss $\Omega_{s,m}$ in the 1st-hop and $\Omega_{m,d}$ in the 2nd-hop are expressed as $\Omega = \Omega_0 \cdot \left(\frac{d}{d_0}\right)^\alpha$ for $(\Omega, d) = \{(\Omega_{s,m}, d_{s,m}), (\Omega_{m,d}, d_{m,d})\}$. Similarly, the path-loss $\Omega_{s,d}$ in the direct channel is formulated as $\Omega_{s,d} = \Omega_0 \cdot \left(\frac{d_{s,d}}{d_0}\right)^\alpha + \Omega_{br}$, where Ω_{br} is the extra path-loss imposed by the complicated environment. Simulation parameters in both physical and MAC layers are in line with TABLE I on the next page, unless some parameter changes are particularly mentioned. The parameters of the non-linear energy harvester are set to $a = 132.8$, $b = 0.01181$ and $P_{sat} = 0.02337$ [36]. Relays are distributed at coordinates of the form $(x_r, \pm d_{s,d}(\frac{1}{10} + \frac{1}{2}))$ and $(x_r, \pm\frac{d_{s,d}}{10})$, where $x_r = 1$. All the results are obtained by averaging the randomness incurred by the channels.

A. Convergence of Algorithm

Observe from Fig. 2[2] that our iterative design can quickly converge after several iterations, when different downlink

[1]It is equivalent to a case, where there is no direct link between the source and the destination in our cooperative network. Therefore, the sub-problem (P2-1) for the transmit beamforming design of the source node can be reformulated as the expression in Line 3 of Algorithm 3. It is a classical semi-definite programming, which can be optimally solved by any convex optimisation tool. Besides, its optimal solution satisfies $\overline{\mathbf{W}}_s(1) = \overline{\mathbf{W}}_s(2) = \cdots = \overline{\mathbf{W}}_s(L)$

[2]Since we focus on the convergence of the iterative algorithm in Fig. 2, the relay selection $m^\ddagger$ and the information decoding index $\boldsymbol{\beta}_{m^\ddagger}$ are traversed. The e2e throughput performance is then averaged by using all feasible solutions.

TABLE I
PARAMETER SETTING

Parameter	Denotation	Value
Number of source's antennas	N_s	2
Number of relays' antennas	N_r	2
Path-loss reference distance	d_0	1 m
Extra path-loss	Ω_{br}	80 dB
Number of transmission frames	L	4
Channel variation coefficients	σ^2	0.01
Number of relays	M	4
Channel factors	λ	0.99
Transmit power of source	P_s	1 W
SNR predefined threshold	$\gamma_{m,th}$	16 dB
Additive noise power	σ_m^2, σ_d^2	-50 dBm
Decoding cost factor	f_{dc}	10^{-3} [14]
Path-loss at reference distance	Ω_0	30 dB
Distance between source and destination	$d_{s,d}$	10 m
Rician factor	K_r	5 [12]

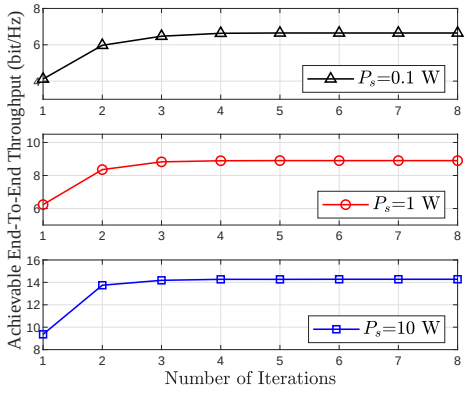

Fig. 2. Convergence of the iterative algorithm with the transmit beamforming design $\mathbf{W}_s(l)$ of the source node as well as the transmit power $\mathbf{P}_{m^\ddagger}$ and power splitter $\boldsymbol{\rho}_{m^\ddagger}$ design of the relay $m^\ddagger$.

transmit power $P_s = \{0.1, 1, 10\}$ W of the source node are considered. Specifically, when we have $P_s = 0.1$ and 1 W, the e2e throughput R_{e2e} in Fig. 2 converges to 6.64 and 8.90 bit/Hz, respectively, after 5 iterations. Moreover, it converges to 14.27 bit/Hz after 4 iterations when $P_s = 10$ W.

B. Transmit Power

We investigate the impact of the source's transmit power on the downlink e2e throughput by setting λ and σ^2 as 0.9 and 1, respectively. Specifically, Fig. 3 (a) demonstrates the throughput performance of the SWIPT-CCN with different relay selection strategies. PRS is compared with the following three relay selection strategies:

- *Max-Min Relay Selection (MMRS):* The relay selection is dominated by the lower SNR between the 1st-hop and the 2nd-hop [37]. We have $m^\ddagger = \arg\max_{m=1,\cdots,M} \min\{\gamma_m(1), \gamma_{m,d}(1)\}$, where $\gamma_{m,d}(1)$ expresses the SNR of the signal received by the destination node during the first TF.
- *Exhaustive Relay Selection (ERS):* All relays are traversed to obtain the optimal one, which has a high complexity.

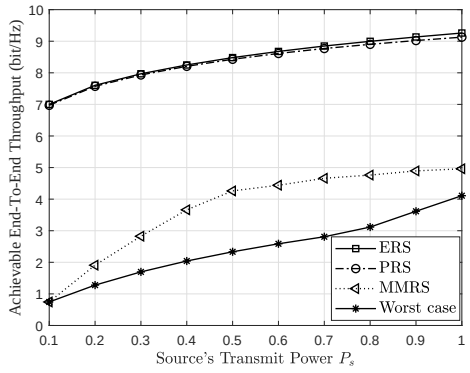

(a)

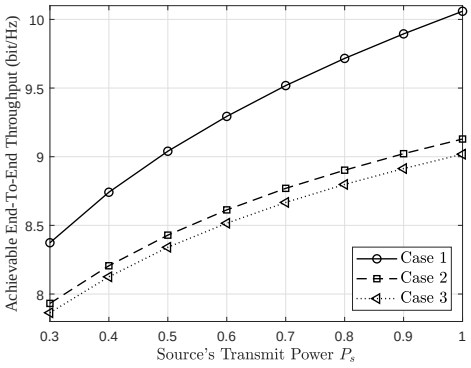

(b)

Fig. 3. Impact of the transmit power on average e2e throughput (a) with different relay selection strategies and (b) with different channel models.

- *Worst Case:* We obtain the relay with the worst performance to be the forwarder.

Observe from Fig. 3 (a) that when we increase P_s, the downlink e2e throughputs of all the relay selection strategies are substantially increased. This is because, as we initially increase the source's transmit power P_s, the relays may gain more energy and higher SNR from the downlink SWIPT. Therefore, they harvest a higher amount of energy for powering their own downlink WIT, while they also obtain a higher successful decoding probability. Moreover, the SNR of the signal in the direct link is also increased. Observe from Fig. 3 (a) that our system with PRS outperforms that with MMRS and the former almost obtains the throughput performance of the ERS. This is because the 1st-hop transmission is critical for the energy-limited relay, which determines the amount of energy harvested and the information decoding.

We plot the SWIPT-CCN with different channel models in Fig. 3 (b). Specifically, three cases are compared, which are detailed as follows:

- *Case 1:* We assume ideal channel conditions in the SWIPT-CCN. Specifically, the CSI does not age within a single transmission cycle.
- *Case 2:* The aging channel is considered. The joint design is obtained based on the accurate CSI of the first frame in the transmission cycle as well as on the knowledge of

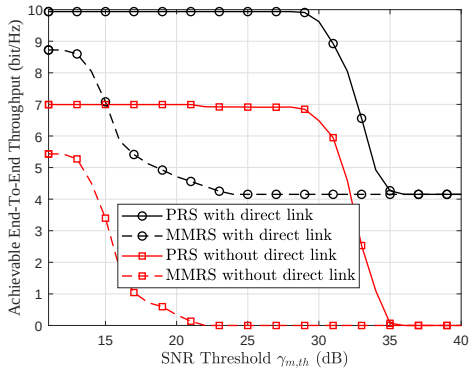

Fig. 4. Impact of the decoding SNR threshold on average achievable e2e throughput.

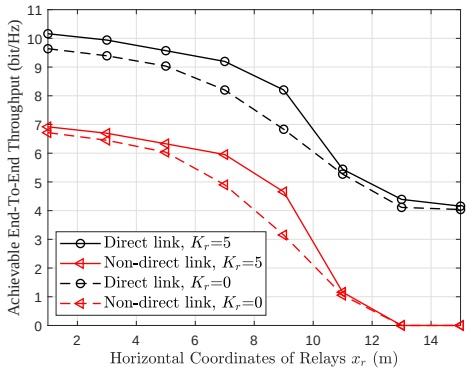

Fig. 5. Impact of distance among relays on average e2e throughput.

the channel aging effect.

- *Case 3:* The aging channel is considered. However, the source only obtains the accurate CSI of the very first transmission frame within a single transmission cycle, while it does not have the aging knowledge of the channel.

In Fig. 3 (b), Case 1 obtains the largest e2e throughput. This is because the ideal CSI improves the SNR of the signal in the SWIPT-CCN. However, it is impractical owing to the time-varying channel conditions. Therefore, the system with real-time aging channels is demonstrated as Case 2 in Fig. 3 (b). Observe from Fig. 3 (b) that Case 2 outperforms Case 3. Therefore, we can obtain the larger throughput in the SWIPT-CCN when we invoke the proposed algorithm by considering the aging channel.

C. Decoding SNR Threshold

We then investigate the impact of the decoding SNR threshold $\gamma_{m,th}$ on the e2e throughput of the CCN with/without the direct link. Observe from Fig. 4 that the downlink e2e throughput of the two scenarios stabilises and then reduces, as we increase $\gamma_{m,th}$. This is because increasing $\gamma_{m,th}$ reduces the forwarding opportunities of the relays, which results in a decreasing throughput. However, as we continuously increase the threshold $\gamma_{m,th}$, all the relays cannot operate WIT at all. Hence, the throughput no longer changes. Specifically, the throughput of our CCN without direct link drops to zero, while that of the CCN with direct link reduces and stabilises.

D. Distance among Relays

Fig. 5 demonstrates the impact of the horizontal coordinates of the relays on the average e2e throughput. Observe from Fig. 5 that as we increase x_r, the throughput first decreases and then trends to be stable. This is because increasing path loss results in the uncorrect decoding at the relays. Therefore, the relays cannot forward any information at all. Note that the CCN without direct link achieves zero throughput, which is coincident with Fig. 4.

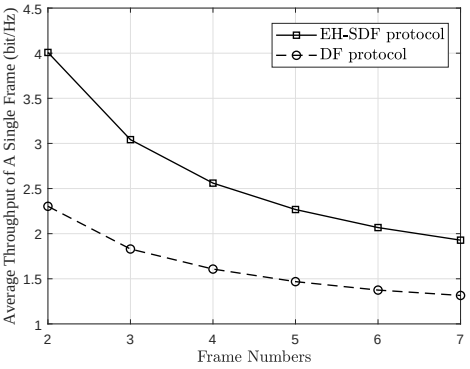

Fig. 6. Impact of transmission frame numbers on average e2e throughput in the scenario with an EH-SDF and a DF protocols.

E. Transmission Frames

Fig. 6 depicts the impact of the number of TFs L on the average downlink e2e throughput per frame. Observe from Fig. 6 that the e2e throughput performance reduces as we increase L in a transmission cycle, which is incurred by the outdated CSI in aging channels. Moreover, we compare the e2e throughput performance between the CCN with an EH-SDF protocol and that with a classical DF protocol. Specifically, the former one achieves better throughput performance than the latter.

VI. Conclusion

We studied a SWIPT-CCN, where wireless powered relays with an EH-SDF protocol adopt power splitters to harvest energy from downlink RF signals emitted by a source for decoding and forwarding the information to the destination. By considering the channel aging, we maximise the e2e throughput of our system by jointly designing relay selection, power allocation and signal splitting of relays as well as transmit beamforming of relays and the source. An iterative joint design is proposed for solving the original non-convex optimisation problem. Numerical results demonstrate the PRS strategy almost achieves the same performance with the optimal strategy, while validating the superiority of the EH-SDF protocol to the DF protocol. Furthermore, we also evaluate the impact of the outdated CSI on the e2e throughput.

Appendix A
Proof of Lemma 1

In the constraint Eq. (19), the derivative of $\Gamma(W)$ with respect to W can be formulated as

$$f(x) \triangleq \frac{\mathrm{d}\Gamma(W)}{\mathrm{d}W} = \frac{\kappa_1 x}{(1+x)^2} - \frac{\kappa_2}{4}, \tag{27}$$

where we define $x \triangleq e^{ab - \frac{W a \lambda^{2(l_i^{\sharp}-1)} \rho_{m_i^{\sharp}}^{\sharp}(l_i^{\sharp}) P_s}{\Omega_{s,m}}}$ for $x \in (0, e^{ab}]$. Note that x is monotonously decreasing with respect to W. By letting $\frac{\mathrm{d}\Gamma(W)}{\mathrm{d}W} = 0$, Eq. (27) can be simplified as $f'(x) \triangleq -\frac{\kappa_2}{4}x^2 + (\kappa_1 - \frac{\kappa_2}{2})x - \frac{\kappa_2}{4} = 0$. Obviously, $f'(x)$ is a concave univariate quadratic function. Therefore, the number of zero point(s) of $f(x)$ can be obtained by $\kappa_1(\kappa_1 - \kappa_2)$. Furthermore, the second-order derivative of $\Gamma(W)$ can be formulated as $\frac{\mathrm{d}^2\Gamma(W)}{\mathrm{d}W^2} = \frac{\kappa_1(1-x)}{(1+x)^3}$. Therefore, in the range of $x < 1$, $f(x)$ is monotonously increasing; otherwise, $f(x)$ is monotonously decreasing. As a result, the range of W satisfying Eq. (19) can be discussed in the following several cases.

In the case of $\kappa_1(\kappa_1 - \kappa_2) < (=)\ 0$, $f'(x) = 0$ has no solution (only has one solution). Therefore, we have $f(x) \leq 0$, which demonstrates the decreasing monotonicity of $\Gamma(W)$. As a result, (P2-1) has no solution when we have $\Gamma(0) < 0$, while the constraint Eq. (19) can be reformulated as $0 \leq W \leq W_{2(0,\infty)}$ when we have $\Gamma(0) \geq 0$, where $W_{2(0,\infty)}$ obtained by bisection method based Algorithm 1 is a unique zero point of $\Gamma(W)$.

In the other case, since we have $\kappa_1(\kappa_1 - \kappa_2) > 0$, $f(x)$ has two different zero points x_1 and x_2 satisfying $x_1 < x_2$. It can be further obtained that $x_1 > 0$. Specifically, we have $\kappa_3 < 0$ owing to $\kappa_1 > 0$, $\kappa_2 > 0$ and $\kappa_1 - \kappa_2 > 0$. Furthermore, we have $|\kappa_3| > \sqrt{\kappa_3^2 - \kappa_2^2/4}$, which results in $x_1 > 0$. The range of W satisfying Eq. (19) is further discussed in the following cases A, B and C.

- In case A of $e^{ab} \leq x_1 < x_2$, we have $f(x) \leq 0$ in the range of $x \in (0, e^{ab}]$. Therefore, $\Gamma(W)$ is monotonously decreasing. It is further discussed in two cases, as shown in Lines 1-2 of Eq. (21), which is similar to the case of $\kappa_1(\kappa_1 - \kappa_2) < (=)\ 0$.
- In case B of $0 < x_1 \leq e^{ab} \leq x_2$, $\Gamma(W)$ has a unique maximum extremum $\Gamma(\omega_1)$. By discussing the positive and negative of $\Gamma(0)$ and $\Gamma(\omega_1)$, the case B is further separated into three cases, as indicated in lines 3-5 of Eq. (21).
- We have $0 < x_1 < x_2 < e^{ab}$ in case C. $\Gamma(W)$ has a maximum extremum ω_1 and a minimum extremum ω_2. Specifically, it is a decreasing-then-increasing-then-decreasing function in $W \in [0, \infty)$. Similar to case B, case C is divided into five sub-cases, as shown in lines 6-10 of Eq. (21), by discussing the positive and negative values of $\Gamma(0)$, $\Gamma(\omega_1)$ and $\Gamma(\omega_2)$.

Lemma 1 is proved.

Appendix B
Proof of Lemma 2

Observe from Eq. (14) that as $\gamma_{m,d}(l)$ increases, the achieved e2e throughput increases. According to the SNR $\gamma_{m,d}(l)$ in Eq. (11), its derivative can be expressed as $\Upsilon \triangleq \frac{\partial \gamma_{m,d}(l)}{\partial P_m(l)} = \frac{\lambda_{m,d}^{2(l-1)} \|\mathbf{h}_{m,d}(1)\|^2 \Omega_{m,d}\sigma_d^2}{\left(\left(1-\lambda_{m,d}^{2(l-1)}\right)\sigma_{m,d}^2 P_m(l) + \Omega_{m,d}\sigma_d^2\right)^2}$. By defining $t \triangleq \lambda_{m,d}^{l-1}$ $(1 \geq \lambda_{m,d} \geq 0)$, we have $\frac{\partial \Upsilon}{\partial t} \geq 0$. Therefore, Υ is a monotonically increasing function with respect to t. Since t is a monotonically decreasing function with respect to l, Υ degrades when we increase l. Specifically, given a fixed $P_m(l)$, the positive slope of $\gamma_{m,d}(l)$ with respect to $P_{m,d}(l)$ decreases, as l increases. Therefore, by consuming the same energy, the relay obtains higher throughput in the earlier TF rather than the later one. Moreover, the SNR in the 1st-hop transmission is generally higher than that in the forwarding one for the energy-limited relay. As a result, the relay may consume all its stored energy to forward the information in the current TF. *Lemma 2* is proved.

References

[1] L. Chettri and R. Bera, "A comprehensive survey on internet of things (IoT) toward 5g wireless systems," *IEEE Internet Things J.*, vol. 7, no. 1, pp. 16–32, 2020.

[2] T. M. Hoang *et. al*, "On the performance of MIMO full-duplex relaying system with SWIPT under outdated CSI," *IEEE Trans. Veh. Technol.*, vol. 69, no. 12, pp. 15 580–15 593, 2020.

[3] J. Hu, X. Cai, and K. Yang, "Joint trajectory and scheduling design for UAV aided secure backscatter communications," *IEEE Wireless Commun. Lett.*, vol. 9, no. 12, pp. 2168–2172, 2020.

[4] J. Hu, K. Yang, G. Wen, and L. Hanzo, "Integrated data and energy communication network: A comprehensive survey," *IEEE Commun. Surveys Tuts.*, vol. 20, no. 4, pp. 3169–3219, Fourthquarter 2018.

[5] J. Hu, Y. Zhao, and K. Yang, "Modulation and coding design for simultaneous wireless information and power transfer," *IEEE Commun. Mag.*, vol. 57, no. 5, pp. 124–130, May 2019.

[6] J. He, V. Tervo, X. Zhou, X. He, S. Qian, M. Cheng, M. Juntti, and T. Matsumoto, "A tutorial on lossy forwarding cooperative relaying," *IEEE Commun. Surveys Tuts.*, vol. 21, no. 1, pp. 66–87, 2019.

[7] A. Agarwal *et. al*, "Finite blocklength non-orthogonal cooperative communication relying on SWIPT-enabled energy harvesting relays," *IEEE Trans. Commun.*, vol. 68, no. 6, pp. 3326–3341, 2020.

[8] J. Guo, S. Zhang, N. Zhao, and X. Wang, "Performance of SWIPT for full-duplex relay system with co-channel interference," *IEEE Trans. Veh. Technol.*, pp. 1–1, 2019.

[9] A. Gupta, K. Singh, and M. Sellathurai, "Time-switching EH-based joint relay selection and resource allocation algorithms for multi-user multi-carrier AF relay networks," *IEEE Trans. Green Commun. and Networking*, vol. 3, no. 2, pp. 505–522, June 2019.

[10] S. Guo *et. al*, "Energy-efficient resource allocation in SWIPT cooperative wireless networks," *IEEE Systems J.*, pp. 1–12, 2020.

[11] M. Oshaghi and M. j. Emadi, "Throughput maximization of a hybrid EH-SWIPT relay system under temperature constraints," *IEEE Trans. Veh. Technol.*, pp. 1–1, 2019.

[12] S. Wang, Z. He, and Y. Rong, "Joint transceiver optimization for DF multicasting MIMO relay systems with wireless information and power transfer," *IEEE Trans. Commun.*, vol. 69, no. 7, pp. 4953–4967, 2021.

[13] Y. Hu, Y. Zhu, M. C. Gursoy, and A. Schmeink, "SWIPT-enabled relaying in IoT networks operating with finite blocklength codes," *IEEE J. Sel. Areas Commun.*, vol. 37, no. 1, pp. 74–88, Jan 2019.

[14] M. Abedi, H. Masoumi, and M. J. Emadi, "Power splitting-based SWIPT systems with decoding cost," *IEEE Wireless Commun. Lett.*, vol. 8, no. 2, pp. 432–435, April 2019.

[15] H. K. Sahu and P. R. Sahu, "SSK-based SWIPT with AF relay," *IEEE Commun. Lett.*, vol. 23, no. 4, pp. 756–759, April 2019.

[16] C. Peng, F. Li, and H. Liu, "Optimal power splitting in two-way decode-and-forward relay networks," *IEEE Commun. Lett.*, vol. 21, no. 9, pp. 2009–2012, 2017.

[17] R. Shankar *et. al*, "Outage probability analysis of selective-decode and forward cooperative wireless network over time varying fading channels with node mobility and imperfect CSI condition," in *TENCON 2018 - 2018 IEEE Region 10 Conf.*, Oct 2018, pp. 0508–0513.

[18] J. Zheng, J. Zhang, E. Bjornson, and B. Ai, "Impact of channel aging on cell-free massive MIMO over spatially correlated channels," *IEEE Trans. Wireless Commun.*, vol. 20, no. 10, pp. 6451–6466, 2021.

[19] X. Chen, Y. Liu, L. X. Cai, Z. Chen, and D. Zhang, "Resource allocation for wireless cooperative IoT network with energy harvesting," *IEEE Trans. Wireless Commun.*, vol. 19, no. 7, pp. 4879–4893, 2020.

[20] X. Li *et. al*, "Robust secure beamforming for SWIPT-aided relay systems with full-duplex receiver and imperfect CSI," *IEEE Trans. Veh. Technol.*, vol. 69, no. 2, pp. 1867–1878, 2020.

[21] Y. Liu, Z. Wen, N. C. Beaulieu, D. Liu, and X. Liu, "Power allocation for SWIPT in full-duplex AF relay interference channels using game theory," *IEEE Commun. Lett.*, vol. 24, no. 3, pp. 608–611, 2020.

[22] Y. Zheng, J. Hu, and K. Yang, "Average age of information in wireless powered relay aided communication network," *IEEE Internet Things J.*, vol. 9, no. 13, pp. 11 311–11 323, 2022.

[23] G. A. Ropokis and P. S. Bithas, "Wireless powered relay networks: Rate optimal and power consumption-aware WPT/SWIPT," *IEEE Trans. Veh. Technol.*, vol. 71, no. 8, pp. 8574–8590, 2022.

[24] J. Laneman, D. Tse, and G. Wornell, "Cooperative diversity in wireless networks: Efficient protocols and outage behavior," *IEEE Trans. Info. Theory*, vol. 50, no. 12, pp. 3062–3080, 2004.

[25] H. Alves and R. D. Souza, "Selective decode-and-forward using fixed relays and packet accumulation," *IEEE Commun. Lett.*, vol. 15, no. 7, pp. 707–709, 2011.

[26] M. Bouteggui *et. al*, "A joint antenna and path selection for MIMO cooperative communication with single selective decode and forward relay," in *2019 International Conf. Wireless Networks and Mobile Commun. (WINCOM)*, 2019, pp. 1–5.

[27] Y. Yao and J. Wen, "SEP performance for selective decode-and-forward cooperative communications over satellite-terrestrial wireless networks," in *2019 International Conference on Intelligent Computing and its Emerging Applications (ICEA)*, 2019, pp. 151–155.

[28] M. Medard, "The effect upon channel capacity in wireless communications of perfect and imperfect knowledge of the channel," *IEEE Trans. Info. Theory*, vol. 46, no. 3, pp. 933–946, 2000.

[29] B. Clerckx *et. al*, "Fundamentals of wireless information and power transfer: From RF energy harvester models to signal and system designs," *IEEE J. Sel. Areas Commun.*, vol. 37, no. 1, pp. 4–33, Jan 2019.

[30] C. Liu *et. al*, "Simultaneous wireless information and power transfer under different CSI acquisition schemes," *IEEE Trans. Wireless Commun.*, vol. 14, no. 4, pp. 1911–1926, April 2015.

[31] B. Su, Q. Ni, and W. Yu, "Robust transmit beamforming for SWIPT-enabled cooperative NOMA with channel uncertainties," *IEEE Trans. Commun.*, vol. 67, no. 6, pp. 4381–4392, 2019.

[32] G. Zhang, Q. Wu, M. Cui, and R. Zhang, "Securing UAV communications via joint trajectory and power control," *IEEE Trans. Wireless Commun.*, vol. 18, no. 2, pp. 1376–1389, 2019.

[33] V. N. Q. Bao *et. al*, "Performance analysis of partial relay selection networks with short packet communications," in *2019 6th NAFOSTED Conf. on Information and Computer Science (NICS)*, 2019, pp. 23–26.

[34] S. X. Wu, W. Ma, and A. M. So, "Physical-layer multicasting by stochastic transmit beamforming and alamouti space-time coding," *IEEE Transactions on Signal Processing*, vol. 61, no. 17, pp. 4230–4245, 2013.

[35] F. Zhao *et. al*, "On the capacity of wireless powered communication systems over Rician fading channels," *IEEE Trans. Commun.*, vol. 66, no. 1, pp. 404–417, 2018.

[36] J. Hu, Y. Zheng, and K. Yang, "Multi-domain resource scheduling for full-duplex aided wireless powered communication network," *IEEE Trans. Veh. Technol.*, pp. 1–13, 2022.

[37] M. Xie, J. Gong, and X. Ma, "Age and energy tradeoff for short packet based two-hop decode-and-forward relaying networks," in *2021 IEEE Wireless Commun. and Networking Conf. (WCNC)*, 2021, pp. 1–6.

Yali Zheng is currently pursuing the Ph.D. degree in the School of Information and Communication Engineering, University of Electronic Science and Technology of China, Chengdu, China. Her current research interests include wireless power communication networks, data and energy integrated communication networks, resource scheduling and age of information.

Jie Hu [S'11, M'16, SM'21] (hujie@uestc.edu.cn) received his B.Eng. and M.Sc. degrees from Beijing University of Posts and Telecommunications, China, in 2008 and 2011, respectively, and received the Ph.D. degree from the School of Electronics and Computer Science, University of Southampton, U.K., in 2015. Since March 2016, he has been working with the School of Information and Communication Engineering, University of Electronic Science and Technology of China (UESTC). He is now a Research Professor and PhD supervisor. He won UESTC's Academic Young Talent Award in 2019. Now he is supported by the "100 Talents" program of UESTC. He is an editor for *IEEE Wireless Communications Letters*, *IEEE/CIC China Communications* and *IET Smart Cities*. He serves for *IEEE Communications Magazine*, *Frontiers in Communications and Networks* as well as *ZTE communications* as a guest editor. He is a technical committee member of ZTE Technology. He is a program vice-chair for IEEE TrustCom 2020, a technical program committee (TPC) chair for IEEE UCET 2021 and a program vice-chair for UbiSec 2022. He also serves as a TPC member for several prestigious IEEE conferences, such as IEEE Globecom/ICC/WCSP and etc. He has won the best paper award of IEEE SustainCom 2020 and the best paper award of IEEE MMTC 2021. His current research focuses on wireless communications and resource management for B5G/6G, wireless information and power transfer as well as integrated communication, computing and sensing.

Kun Yang [M'00, SM'10, F'23] received his PhD from the Department of Electronic & Electrical Engineering of University College London (UCL), UK. He is a Chair Professor in the School of Computer Science & Electronic Engineering, University of Essex, leading the Network Convergence Laboratory (NCL), UK. He is also an affiliated professor at UESTC, China. Before joining in the University of Essex at 2003, he worked at UCL on several European Union (EU) research projects for several years. His main research interests include wireless networks and communications, IoT networking, data and energy integrated networks and mobile computing. He manages research projects funded by various sources such as UK EPSRC, EU FP7/H2020 and industries. He has published 400+ journal papers and filed 20 patents. He serves on the editorial boards of both IEEE (e.g., IEEE TNSE, WCL, ComMag) and non-IEEE journals. He is an IEEE ComSoC Distinguished Lecturer (2020-2021) and a Member of Academia Europaea (MAE).